A&A 677, L2 (2023)
https://doi.org/10.1051/0004-6361/202346128

Astronomy & Astrophysics

LETTER TO THE EDITOR

The peak flux of GRB 221009A measured with GRBAlpha

Jakub Řípa[1], Hiromitsu Takahashi[2], Yasushi Fukazawa[2], Norbert Werner[1], Filip Münz[1], András Pál[3], Masanori Ohno[2], Marianna Dafčíková[1], László Mészáros[3], Balázs Csák[3], Nikola Husáriková[1], Martin Kolář[1], Gábor Galgóczi[4,5], Jean-Paul Breuer[1], Filip Hroch[1], Ján Hudec[6], Jakub Kapuš[6], Marcel Frajt[6], Maksim Rezenov[6], Robert Laszlo[7], Martin Koleda[7], Miroslav Šmelko[8,9], Peter Hanák[9], Pavol Lipovský[9], Tomáš Urbanec[10], Miroslav Kasal[10], Aleš Povalač[10], Yuusuke Uchida[11], Helen Poon[2], Hiroto Matake[2], Kazuhiro Nakazawa[12], Nagomi Uchida[13], Tamás Bozóki[14], Gergely Dálya[15], Teruaki Enoto[16], Zsolt Frei[4], Gergely Friss[4], Yuto Ichinohe[17], Kornél Kapás[18,19,5], László L. Kiss[3], Tsunefumi Mizuno[2], Hirokazu Odaka[20], János Takátsy[4,5], Martin Topinka[21], and Kento Torigoe[2]

(Affiliations can be found after the references)

Received 12 February 2023 / Accepted 14 March 2023

ABSTRACT

Context. On 2022 October 9 the brightest gamma-ray burst (GRB) ever observed lit up the high-energy sky. It was detected by a multitude of instruments, attracting the close attention of the GRB community, and saturated many detectors.
Aims. GRBAlpha, a nano-satellite with a form factor of a 1U CubeSat, detected this extraordinarily bright long-duration GRB, GRB 221009A, without saturation but affected by pile-up. We present light curves of the prompt emission in 13 energy bands, from 80 keV to 950 keV, and performed a spectral analysis to calculate the peak flux and peak isotropic-equivalent luminosity.
Methods. Since the satellite's attitude information is not available for the time of this GRB, more than 200 incident directions were probed in order to find the median luminosity and its systematic uncertainty.
Results. We find that the peak flux in the 80−800 keV range (observer frame) was $F_{\rm ph}^{\rm p} = 1300^{+1200}_{-200}$ ph cm^{-2} s^{-1}, or $F_{\rm erg}^{\rm p} = 5.7^{+3.7}_{-0.7}\times10^{-4}$ erg cm^{-2} s^{-1}, and the fluence in the same energy range of the first GRB episode, which lasted 300 s and was observable by GRBAlpha, was $S = 2.2^{+1.4}_{-0.3} \times 10^{-2}$ erg cm^{-2}, or $S^{\rm bol} = 4.9^{+0.8}_{-0.5} \times 10^{-2}$ erg cm^{-2} for the extrapolated range of 0.9−8690 keV. We infer the isotropic-equivalent released energy of the first GRB episode to be $E_{\rm iso}^{\rm bol} = 2.8^{+0.8}_{-0.5} \times 10^{54}$ erg in the 1−10 000 keV band (rest frame at $z = 0.15$). The peak isotropic-equivalent luminosity in the 92−920 keV range (rest frame) was $L_{\rm iso}^{\rm p} = 3.7^{+2.5}_{-0.5} \times 10^{52}$ erg s^{-1}, and the bolometric peak isotropic-equivalent luminosity was $L_{\rm iso}^{\rm p,bol} = 8.4^{+2.5}_{-1.5} \times 10^{52}$ erg s^{-1} (4 s scale) in the 1−10 000 keV range (rest frame). The peak emitted energy is $E_{\rm p}^{*} = E_{\rm p}(1+z) = 1120 \pm 470$ keV. Our measurement of $L_{\rm iso}^{\rm p,bol}$ is consistent with the Yonetoku relation. It is possible that, due to the spectral evolution of this GRB and the orientation of GRBAlpha at the peak time, the true values of peak flux, fluence, $L_{\rm iso}$, and $E_{\rm iso}$ are even higher.

Key words. gamma-ray burst: individual: GRB 221009A

1. Introduction

On 2022 October 9 at 13:16:59.988 UT, the *Fermi* Gamma-ray Burst Monitor (GBM) detected the exceptionally bright long gamma-ray burst (GRB) GRB 221009A (Veres et al. 2022; Lesage et al. 2022, 2023). The burst was also observed by the *Fermi* Large Area Telescope (LAT) up to the energy of 100 GeV (Pillera et al. 2022). Potentially remarkable detections of over 5000 very high-energy photons with energies up to 18 TeV were reported by the Large High Altitude Air Shower Observatory (LHAASO; Huang et al. 2022), and a possible 251 TeV photon was reported by Carpet-2 (Dzhappuev et al. 2022), triggering the interest of the broader physics community.

The burst was localised by the *Neil Gehrels Swift* Observatory's Burst Alert Telescope (Dichiara et al. 2022) and followed up by the Very Large Telescope (VLT) X-shooter instrument (de Ugarte Postigo et al. 2022; Malesani et al. 2023), which determined that it occurred at a redshift of 0.151 and belongs to very near long GRBs (Oates 2023). It was also detected by a multitude of other instruments: AGILE/GRID (Piano et al. 2022), AGILE/MCAL (Ursi et al. 2022), BepiColombo/MGNS (Kozyrev et al. 2022), Insight-HXMT and SATech-01/GECAM-C (HEBS; An et al. 2023), INTEGRAL/SPI-ACS (Gotz et al. 2022), Konus-WIND & SRG/ART-XC (Frederiks et al. 2023), MAXI and NICER (Williams et al. 2023), Solar Orbiter/STIX (Xiao et al. 2022), STPSat-6/SIRI-2 (Mitchell et al. 2022), and *XMM-Newton* (Tiengo et al. 2023).

This brightest ever recorded GRB (Burns et al. 2023; O'Connor et al. 2023) saturated many of the GRB detectors in orbit, hampering the efforts to determine its peak luminosity. In this Letter, we present the peak flux and peak isotropic-equivalent luminosity of this extraordinary transient as measured by the GRBAlpha nano-satellite.

2. GRBAlpha

GRBAlpha (Pál et al. 2020) is a 1U CubeSat carrying a GRB detector as a technology demonstration for an envisioned future CubeSat constellation (Werner et al. 2018; Mészáros et al. 2022). It was launched on 2021 March 22 into a Sun-synchronous

polar orbit at an altitude of ∼550 km and thus became the smallest astrophysical space observatory. About a third of the polar orbit is affected by high particle background, and the duty cycle of the detector is around 67%. GRBAlpha's detector consists of a $75 \times 75 \times 5\,\mathrm{mm}^3$ CsI(Tl) scintillator read out by an array of Silicon PhotoMultipliers (SiPMs), called multi-pixel photon counters (MPPCs), by Hamamatsu. The SiPM detectors are protected from proton damage by a 2.5 mm thick lead (PbSb3 alloy) shield, and their degradation is being monitored. The on-board data acquisition software stack is being continuously upgraded to increase the duty cycle and data downlink rate. The ground segment is also supported by the radio amateur community, and it takes advantage of the Satellite Networked Open Ground Station (SatNOGS)[1].

Following a commissioning phase, GRBAlpha started collecting data, monitoring the particle and photon background environment on a low-Earth polar orbit, and detecting transients (see Řípa et al. 2022a). When the satellite operates continuously, on average it detects a transient every 5–6 days[2]. GRBAlpha detected GRB 221009A (Řípa et al. 2022b) when traversing the northern polar regions, and during the peak brightness of the burst its detectors were not saturated; however, the measurement was influenced by pile-up.

The pile-up effect occurs due to the chance coincidence of the arrival and interaction of two or more gamma-ray photons in the detector's scintillator within the detector's inherent resolving time. In that case, two or more events are registered as one event, and the energies of the events within the same resolving time window are added (Knoll 2000).

3. Data analysis

GRBAlpha observed a peak count rate of $22\,000\,\mathrm{cnt\,s^{-1}}$ in the ∼80−950 keV energy band at 13:20:51.5 UTC on 2022 October 9. The duration of the GRB was >250 s (Řípa et al. 2022b). During the detection, the satellite was flying above the northern polar region with elevated background levels. The end part of the GRB was recorded while passing the outer Van Allen radiation belt; therefore, we can only report the lower limit on the duration and cannot determine the T_{90} duration of the GRB. The GRBAlpha data for this event are composed of binned light curves with 4 s temporal resolution recorded in 16 energy bands. However, the three lowest-energy bands are below the set on-board low-energy threshold limited by the noise peak of the MPPCs, making only 13 energy bands suitable for spectral analysis. The recorded raw count-rate curves in multiple energy bands are presented in Fig. 1. We note that the energy calibration was performed by using radionuclides in the laboratory and by observing activation lines in orbit.

We performed spectral analysis to determine the peak flux of the GRB and its isotropic-equivalent peak luminosity. The mass model of GRBAlpha used for generating detector response matrices employed in the spectral analysis is displayed in Fig. 2. It contains: the detector made of a $75 \times 75 \times 5\,\mathrm{mm}^3$ CsI(Tl) scintillator in a 1.5 mm thick Al casing; a 2.5 mm thick PbSb3 radiation shield; a standard 1U CubeSat Al platform with four stacks of empty printed circuit boards (PCBs; glass epoxy FR4) and two $LiFePO_4$ batteries.

A full Monte Carlo simulation based on the GEometry ANd Tracking (Geant4) toolkit[3] (Allison & Amako 2016) was carried out to simulate incident photons with a flat energy distribution in the 5−1000 keV band, covering the entire satellite structure. The deposited energy as a function of input photon energy was calculated by scanning more than 200 incident Θ (zenith) and Φ (azimuth) angles. The effective area versus incident photon energy for a few zenith angles, Θ, and a constant azimuth angle $\Phi = 270°$ is shown in Fig. 3. The drop over 900 keV is an artefact because we simulated photon energies only up to 1000 keV and the photo-absorption peak (with broadening of the energy resolution) of such high-energy photons is not accounted for in this response. Therefore, in the spectral analysis, we conservatively only used data up to ∼810 keV.

To check for pile-up, we plotted the fraction of the detected counts in each spectral band versus the total counts over the whole energy range for GRB 221009A (see Fig. 4). The figure shows that above $\sim 10\,000\,\mathrm{cnt\,bin^{-1}} = 2500\,\mathrm{cnt\,s^{-1}}$ the fraction of counts in the lower-energy bands decreases while the fraction of counts in the higher-energy bands increases, which may indicate the presence of pile-up. We note that below $\sim 10\,000\,\mathrm{cnt\,bin^{-1}}$ the decrease in the rates at high energies as a function of total counts in each bin is due to very low count numbers, and the diagonal lines correspond to 1, 2, 3 . . . $\mathrm{cnt\,bin^{-1}}$. At the peak of this transient, GRBAlpha measured a count rate of $m = 22\,000\,\mathrm{cnt\,s^{-1}}$ in the full band. The shaping parameter of the analogue electronics is $\tau_1 \approx 10\,\mu\mathrm{s}$. During the signal digitisation, the pulse processing is done within the resolution time of $\tau_2 = 15\,\mu\mathrm{s}$. We can calculate the probability that a pile-up appears as (Knoll 2000)

$$P = 1 - e^{-n\tau_2}. \tag{1}$$

Here n is the true event rate, which can be calculated from the detected count rate, m, as

$$n = -\frac{\ln(1 - \mathrm{m}\tau)}{\tau}, \tag{2}$$

where for $m = 22\,000\,\mathrm{cnt\,s^{-1}}$ we obtain $n = 26\,700\,\mathrm{event\,s^{-1}}$. For the observed peak count rate we obtain a pile-up probability of ∼33%, whereas the probability drops to ∼3.7% for a count rate of $m = 2500\,\mathrm{cnt\,s^{-1}}$. Therefore, the observed spectrum at the peak time is affected by pile-up, and in the following spectral analysis we avoid fitting the peak spectrum (which results in a flatter power-law fit) and instead fit the GRB spectrum before the peak time, when the pile-up is negligible.

The spectral fitting was performed by the X-ray spectral fitting package XSPEC[4] (Arnaud 1996). The source spectrum was fitted from time $t_s = 13:20:33.5$ UTC to $t_s + 4$ s, and the background spectrum was taken from time $t_b = 13:17:33.5$ UTC to $t_b + 4$ s. By applying this background, we obtained a background-subtracted spectrum without any substantial bump or dip around 500 keV, where the GRBAlpha background shows a bump. The average background rate in the whole sensitivity range in this part of the orbit is $340\,\mathrm{cnt\,s^{-1}}$, and the rate in the chosen 4 s background bin is $345\,\mathrm{cnt\,s^{-1}}$. We set a systematic error of 2% to be added when evaluating χ^2. The peak time in the measured light curve in the whole sensitivity range of ∼80−950 keV was measured to be from $t_p = 13:20:49.5$ UTC to $t_p + 4$ s. Figure 5 displays the detected count spectra at the time bins t_s, t_b, and t_p. At an approximate time $t_r = \sim 13:24:42.0$ UTC, the GRBAlpha nano-satellite entered the outer Van Allen radiation belt, and the signal from the GRB became flooded by particle background. These times are marked in Fig. 1.

[1] https://satnogs.org
[2] The list of all GRBAlpha-detected transients is available at https://monoceros.physics.muni.cz/hea/GRBAlpha/
[3] https://geant4.web.cern.ch/
[4] https://heasarc.gsfc.nasa.gov/xanadu/xspec/

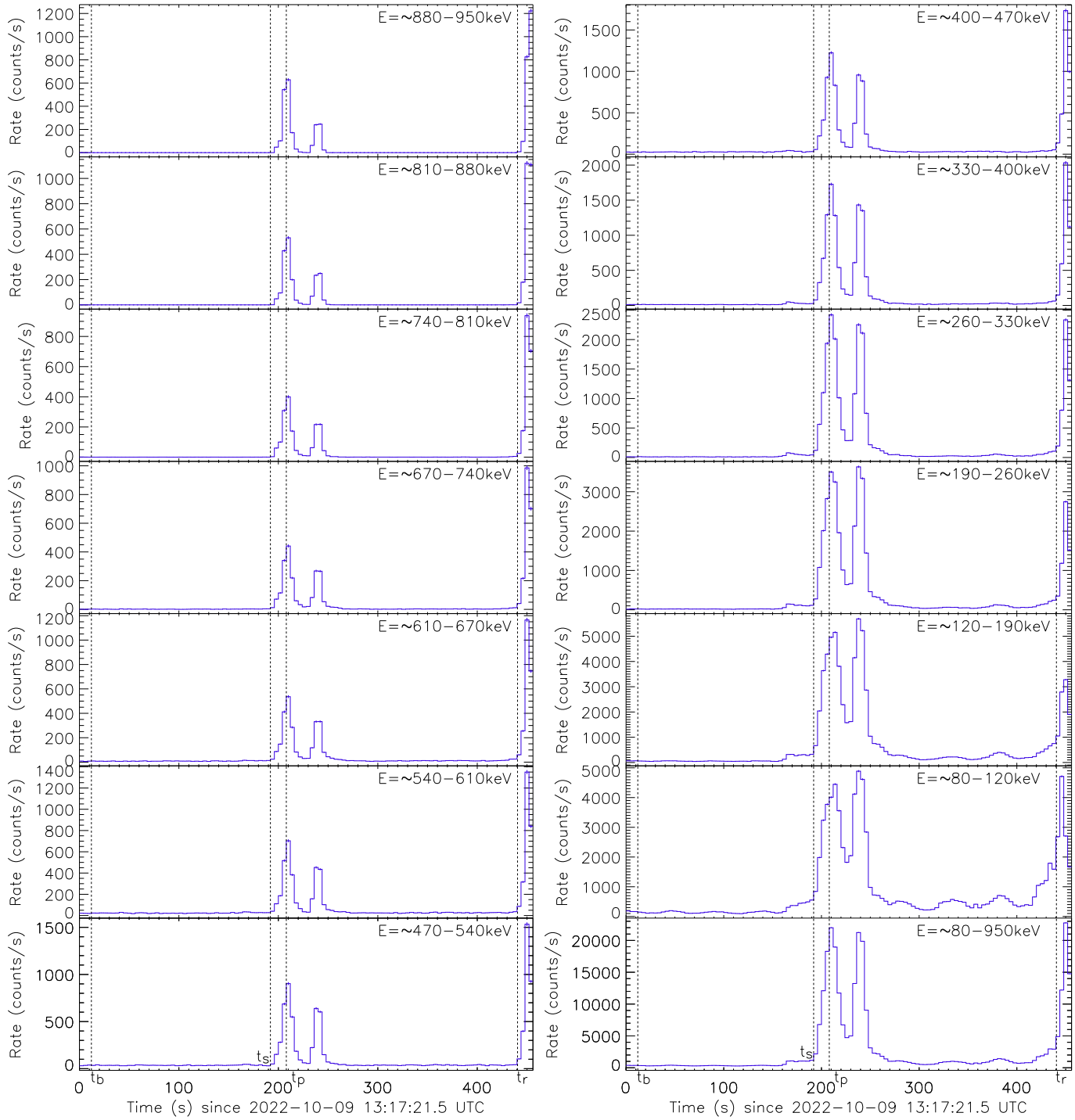

Fig. 1. Raw light curve of GRB 221009A as observed by GRBAlpha in multiple energy bands with 4 s cadence. The bottom-rightmost panel shows the light curve in the whole sensitivity range. Times t_b, t_s, and t_p mark the beginning of the used background interval, the source spectral data, and the peak time, respectively. About 30 s after the peak at t_p, the GRB shows a second strong peak. Time t_r marks the approximate moment when the satellite entered the outer Van Allen radiation belt, which resulted in the final part of the GRB prompt emission being flooded by the particle background. The sharp increase just after t_r is due to this background.

GRBAlpha does not have an active attitude control system, and the attitude knowledge was not being recorded at the time of GRB 221009A. The background variation had a periodicity of ~47 s when the satellite was near the north pole. From the communication with the satellite on the same day, we observed in the radio waterfall a periodicity of ~23 s in the received radio power. The Ultra High Frequency (UHF) antenna on GRBAlpha is a half-wave dipole, and thus a periodicity in the waterfall corresponds to half of the rotation or precession period of the satellite. Hence, the satellite completed more than one revolution during the duration of the GRB. We therefore performed the spectral analysis for many detector response matrices simulated for various Θ and Φ incident angles. We fitted the measured spectra each time in order to obtain the best-fit χ^2 map and to obtain the most likely direction of the GRB with respect to the satellite's coordinate system.

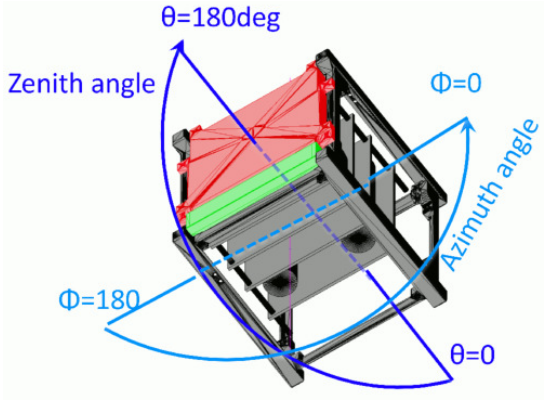

Fig. 2. Mass model of GRBAlpha used for generating detector response matrices, with zenith and azimuth angles marked. The CsI(Tl) detector in its aluminium casing is shown in red and the PbSb3 radiation shield in green. The aluminium CubeSat platform, with four stacks of PCBs and two $LiFePO_4$ batteries, is shown in grey.

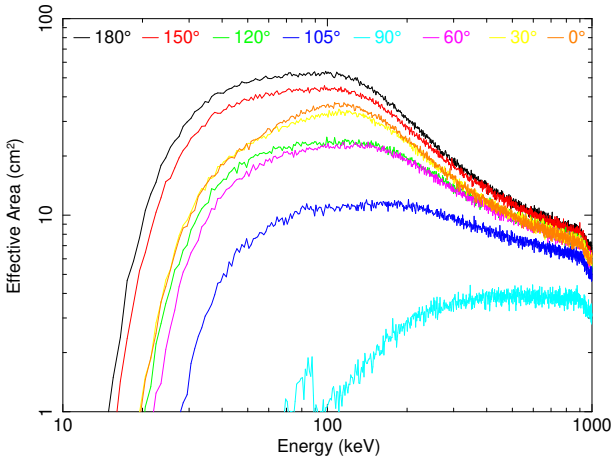

Fig. 3. Total response efficiency (effective area) vs. incident photon energy for a few zenith angles, Θ, and a constant azimuth angle, Φ = 270°.

We performed the spectral fitting with the power-law model, a power law with an exponential cutoff model (CPL), and with the Band function. The lowest reduced χ^2 was obtained for the CPL model, as described in the following section. The reduced χ^2 maps show a similar trend; therefore, in the next section, we report results obtained with the CPL model only.

After we determined the most likely incidence angle of the GRB with respect to the detector, we calculated the flux and the isotropic-equivalent luminosity of the GRB using the best-fit spectral model. Scaling up the flux and the luminosity obtained from the spectral fit at time t_s allowed us to determine the flux and the luminosity at the peak time, t_p. The scaling factor is approximately the ratio of the total detected counts at the time bin t_p over the total detected counts at the time bin t_s. The results are described in detail in the following section.

4. Results

The best fit for the source spectrum at the time bin t_s and after subtraction of the background at the time bin t_b was obtained for

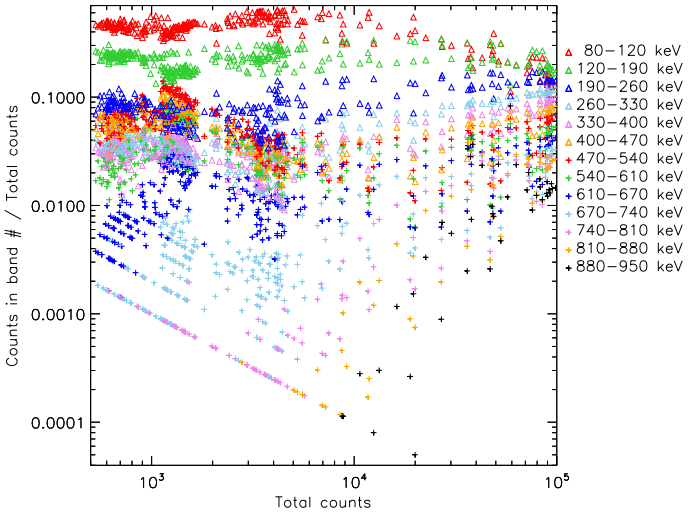

Fig. 4. Fraction of the detected counts in each spectral band vs the total counts over the whole energy range for GRB 221009A and for the background as it passed the north polar region. The counts were detected in 4 s time bins. The figure shows that above ∼10 000 cnt bin = 2500 cnt s^{-1} the fraction of counts in low-energy bands decreases while the fraction of counts in high-energy bands increases, which can indicate a pile-up effect.

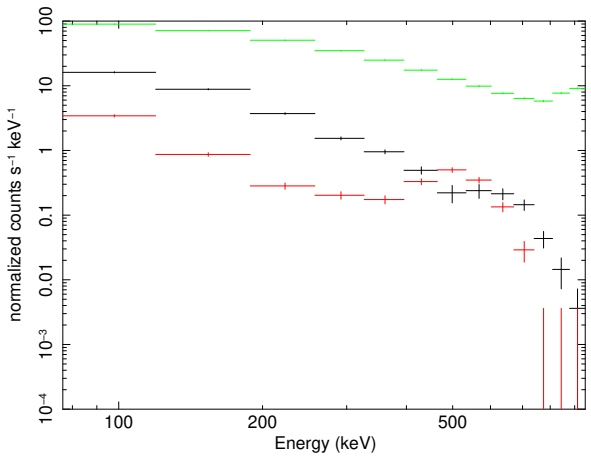

Fig. 5. Detected count spectra of GRB 221009A and the background spectrum. The count spectrum of the GRB at time t_s minus the background spectrum at time t_b is shown in black. The background spectrum at time t_b is shown in red. The count spectrum of the GRB at the peak time t_p = 13:20:49.5 UT on 2022 October 9, minus the background spectrum at time t_b, is shown in green and it reveals a spectral hardening at the highest energies present around the GRB peak.

the on-axis direction Θ = 180° and Φ = 0° by the CPL model:

$$N(E) = A\left(\frac{E}{1\,\mathrm{keV}}\right)^{-\alpha}\exp\left(-\frac{E}{E_0}\right) \tag{3}$$

(see Fig. 6). The fit was performed in the range 76–809 keV, giving χ^2/D.o.F. = 13.4/8 = 1.68. The best-fit parameters are: the photon index $\alpha = 0.7\pm0.1$; the roll-off energy $E_0 = 750^{+410}_{-200}$ keV; and the normalisation $A = 8^{+6}_{-4}$ ph keV^{-1} cm^{-2} s^{-1} at 1 keV. The relatively large uncertainty of the normalisation is due to its correlation with the photon index alpha and the roll-off energy. The 68% confidence interval (CI) parameter uncertainties were calculated by XSPEC from the fit covariance matrix. The peak energy is $E_p = E_0(2-\alpha) = 980 \pm 410$ keV.

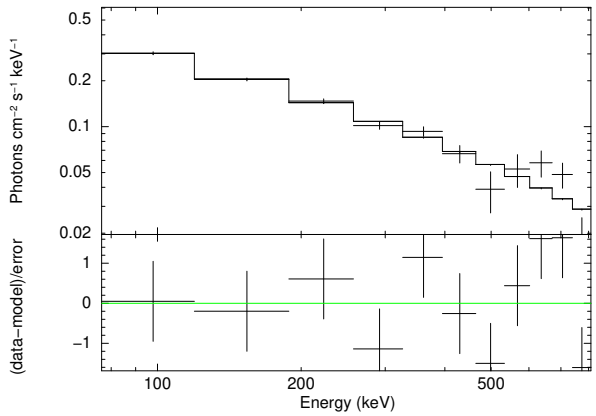

Fig. 6. Spectrum of the GRB 221009A best fit by the CPL model fitted from t_s = 13:20:33.5 UTC on 2022 October 9 to t_s + 4 s in the range 76−809 keV for Θ = 180° and Φ = 0°.

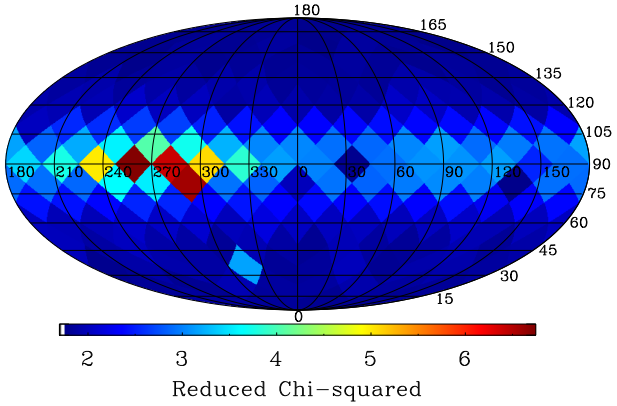

Fig. 7. Reduced χ^2 map of the best fits with the CPL model for different angles of Θ (vertical) and Φ (horizontal) in degrees.

The flux in the energy range of 80−800 keV in the observer frame for the best-fit model for the same time interval t_s and the same Θ and Φ angles was derived to be $F^s_{ph} = 68 \pm 1$ ph cm^{-2} s^{-1}, or $F^s_{erg} = 3.3 \pm 0.1 \times 10^{-5}$ erg cm^{-2} s^{-1} (68% CI). For the isotropic-equivalent luminosity in the energy range 92−920 keV in the rest frame for the redshift $z = 0.151$ (de Ugarte Postigo et al. 2022; Malesani et al. 2023), the cosmological parameter $\Omega_\Lambda = 0.685$, a flat universe, and a Hubble constant of $H_0 = 67.4$ km s^{-1} Mpc^{-1} (Planck Collaboration VI 2020), we obtain $L^s_{iso} = 2.2^{+0.1}_{-0.0} \times 10^{51}$ erg s^{-1} (68% CI). The uncertainties in flux and luminosity were derived from the Markov chain Monte Carlo method (Hastings 1970) with following parameters: a proposal Gaussian fit; the covariance matrix used in the proposal distribution re-scaled by a factor of 0.125; a chain length of 50 000; the first 1000 steps discarded prior to storing the chain; and a Goodman-Weare chain type with 16 walkers.

The approximate scaling factor $f = (C_p - C_b)/(C_s - C_b)$ – the ratio between the total detected counts C_p at the peak time bin t_p minus mean background counts $C_b = 1360$ cnt bin = 340 cnt s^{-1} and the total detected counts C_s at the time bin t_s minus the mean background counts – gives $f = (87\,950 - 1360)/(8689 - 1360) = 11.8$. We scaled the flux and the luminosity obtained from the spectral fit at time t_s by this factor and by the pile-up correction factor of 1.21 in order to determine the flux and the luminosity at the peak time, t_p. By applying this scaling to the flux and the isotropic-equivalent luminosity derived above for the time bin t_s, we obtain for the peak flux $F^p_{ph} = 970 \pm 20$ ph cm^{-2} s^{-1}, or $F^p_{erg} = 4.6 \pm 0.2 \times 10^{-4}$ erg cm^{-2} s^{-1}, and for the peak luminosity $L^p_{iso} = 3.1 \pm 0.1 \times 10^{52}$ erg s^{-1}.

We have so far not considered the systematic uncertainty due to the uncertain attitude of the satellite (detector). Although we derived the most likely orientation of the satellite with respect to the GRB from the best-fit χ^2 map, the difference in reduced χ^2 near the on-axis direction (Θ = 180°) and near the backside direction (Θ = 0°) is relatively low, implying that the on-axis direction is not guaranteed. Therefore, we also calculated the flux and the luminosity using a more conservative approach.

We took the distribution of fluxes and luminosities obtained by fitting the spectra by the CPL model at the same time bin t_s with the same background time bin, t_b, as described above, and used 192 different Θ and Φ directions, which isotropically sample the sphere around the satellite following the Hierarchical Equal Area isoLatitude Pixelization (HEALPix)[5] tessellation (Górski et al. 2005). The best-fit χ^2 was obtained for each direction. The reduced χ^2_r map is shown in Fig. 7. We removed six cases that have reduced $\chi^2_r > 4$ because these we consider as not acceptable fits. They correspond to the direction towards the MPPCs' lead shield. The resulting distribution contains 186 fluxes (luminosities). The median flux in the 80−800 keV range (observer frame) and the isotropic-equivalent luminosity in the 92−920 keV range (rest frame) at the same time bin t_s are: $F^s_{ph} = 94^{+85}_{-17}$ ph cm^{-2} s^{-1}, or $F^s_{erg} = 4.0^{+2.6}_{-0.5} \times 10^{-5}$ erg cm^{-2} s^{-1}; and $L^s_{iso} = 2.6^{+1.7}_{-0.3} \times 10^{51}$ erg s^{-1}.

By applying the scaling factor $f = (C_p - C_b)/(C_s - C_b) = 11.8$ and a pile-up correction factor of 1.21, we obtain for the peak flux $F^p_{ph} = 1300^{+1200}_{-200}$ ph cm^{-2}s^{-1}, or $F^p_{erg} = 5.7^{+3.7}_{-0.7} \times 10^{-4}$ erg cm^{-2} s^{-1}, and for the isotropic-equivalent peak luminosity $L^p_{iso} = 3.7^{+2.5}_{-0.5} \times 10^{52}$ erg s^{-1}. When we repeated this analysis for the fluxes integrated over a larger extrapolated energy range of 0.9−8690 keV, we obtain a peak flux $F^{p,bol}_{erg} = 1.3^{+0.4}_{-0.2} \times 10^{-3}$ erg cm^{-2}s^{-1} and a bolometric isotropic-equivalent peak luminosity $L^{p,bol}_{iso} = 8.4^{+2.5}_{-1.5} \times 10^{52}$ erg s^{-1} (4 s scale) in the 1 − 10 000 keV range (rest frame). Results for the on-axis direction and those obtained by varying different incident directions are summarised in Table 1.

Knowing the peak flux, F^p_{erg}, we can calculate the approximate fluence, S, of the GRB as

$$S = \frac{C - kC_b}{C_p - C_b} F^p_{erg} \Delta t, \quad (4)$$

where C is the total number of detected counts during the GRB, C_p is the number of detected counts at the peak time bin (t_p) of duration $\Delta t = 4$ s, C_b is the mean counts per bin, and k is the number of bins over which we calculate the fluence. We obtain the fluence $S = 2.2^{+1.4}_{-0.3} \times 10^{-2}$ erg cm^{-2} in the 80−800 keV range of the first GRB episode, which lasted 300 s and was observable by GRBAlpha from time 13:19:29.5 to 13:24:29.5 UTC on 2022 October 9. In the same way, but using the wider extrapolated energy range 0.9−8690 keV, we obtain the fluence $S^{bol} = 4.9^{+0.8}_{-0.5} \times 10^{-2}$ erg cm^{-2} and the isotropic-equivalent released energy $E^{bol}_{iso} = 2.8^{+0.8}_{-0.5} \times 10^{54}$ erg in the 1 − 10 000 keV range (rest frame).

5. Discussion

The highest peak flux and fluence of all GRBs recorded with CGRO/BATSE (Paciesas et al. 1999) and *Fermi*/GBM (von Kienlin et al. 2020) are 496 ph cm^{-2} s^{-1} (50−300 keV)

[5] https://healpix.sourceforge.io

Table 1. Summary of obtained fluxes and luminosities for the on-axis direction ($\Theta = 180°$, $\Phi = 0°$), the median values obtained by varying different incident angles, and the values for the edge-on direction ($\Theta = 90°$, $\Phi = 101°$).

Method	$F^{\rm s}_{\rm ph}$ (ph cm^{-2} s^{-1})	$F^{\rm s}_{\rm erg}$ (10^{-5} erg cm^{-2} s^{-1})	$L^{\rm s}_{\rm iso}$ (10^{51} erg s^{-1})	$F^{\rm p}_{\rm ph}$ (ph cm^{-2} s^{-1})	$F^{\rm p}_{\rm erg}$ (10^{-4} erg cm^{-2} s^{-1})	$L^{\rm p}_{\rm iso}$ (10^{52} erg s^{-1})
On-axis	68 ± 1	3.3 ± 0.1	$2.2^{+0.1}_{-0.0}$	970 ± 20	4.6 ± 0.2	3.1 ± 0.1
Median	94^{+85}_{-17}	$4.0^{+2.6}_{-0.5}$	$2.6^{+1.7}_{-0.3}$	1300^{+1200}_{-200}	$5.7^{+3.7}_{-0.7}$	$3.7^{+2.5}_{-0.5}$
Edge-on	390 ± 10	$13.7^{+0.4}_{-0.1}$	$9.1^{+0.3}_{-0.1}$	5600 ± 100	$19.6^{+0.6}_{-0.1}$	$12.9^{+0.4}_{-0.2}$

Notes. The values marked with superscripts 's' and 'p' were derived for the time bin $t_{\rm s}$ and the peak time, $t_{\rm p}$, respectively. Fluxes are for the 80−800 keV range (observer frame), and luminosities are for the 92−920 keV range (rest frame).

and 8.1×10^{-4} erg cm^{-2} (50−300 keV) for GRB 130427A. The measured peak flux and fluence of GRB 221009A are 1020^{+950}_{-160} ph cm^{-2} s^{-1} and $8.3^{+5.3}_{-1.1} \times 10^{-3}$ erg cm^{-2} in the 50−300 keV band. The duration of GRB 221009A is longer than 100 s, compared to the 10−20 s for GRB 130427A, resulting in a relatively large fluence ratio. This indicates that GRB 221009A is indeed exceptionally bright. While the size of the CsI scintillator on GRBAlpha is not small (~55 cm^2 face-on), the low-energy threshold of the detector is relatively high at around 80 keV due to the radiation damage of the SiPM detectors. This allowed GRBAlpha to avoid saturation of the count rate in the digital processing, in turn allowing us to trace the light curve. We note that the brightest gamma-ray flux from a celestial object was observed during the giant flare from the magnetar SGR 1806-20 in 2004; its peak flux was around 10–20 erg s^{-1} in the 20–10 000 keV band (Mazets et al. 2005; Terasawa et al. 2005), which is 4–5 orders of magnitude higher than that of GRB 221009A.

This exceptionally bright GRB has one of the highest isotropic-equivalent peak luminosities ever reported (Burns et al. 2023). Gamma-ray bursts with higher peak luminosities have been observed in the past, but at significantly larger redshifts (see e.g., Yonetoku et al. 2010). In their Fig. 3, Yonetoku et al. 2010 provide the correlation between the rest-frame spectral peak energy and 1-s peak luminosity of short and long GRBs. Our measurements of $L^{\rm p,bol}_{\rm iso} = 8.4^{+2.5}_{-1.5} \times 10^{52}$ erg s^{-1} and $E^{*}_{\rm p} = E_{\rm p}(1+z) = 1120 \pm 470$ keV are consistent with this relation within the systematic errors.

In Fig. 1 one can see that at low energies, mainly at 80−120 keV, the background shows a wavy pattern. This is most likely due to the periodic motion of GRBAlpha that exposes a different cross-section of its detector to the cosmic X-ray background and the secondary gamma-rays induced by cosmic rays in the Earth's atmosphere (Galgóczi et al. 2021). On the same day that we detected this GRB, we also observed a periodicity in the received radio power in the waterfalls while downloading data from the satellite; this indicates that the satellite completed more then one revolution during the duration of the GRB. Therefore, a change in the satellite's attitude between times $t_{\rm s}$ and $t_{\rm p}$ can result in a systematic error of the reported peak luminosity and total emitted energy. As shown in Table 1, the luminosity derived for the edge-on direction is 3.5 times higher than the median value. We cannot exclude that the detector on board GRBAlpha was oriented edge-on towards the GRB at the time of the peak, and therefore, we cannot exclude that the obtained median peak flux and luminosity are underestimated.

The time-resolved spectral analysis of GRB 221009A by Konus-WIND (Frederiks et al. 2023) reveals a spectral evolution during the burst with a higher photon index, α, and the peak energy, $E_{\rm p}$, around the peak time reaching $E_{\rm p} \approx 3$ MeV. Hence, our method based on scaling the flux from the spectrum at time $t_{\rm s}$ to peak time $t_{\rm p}$ may underestimate the resultant peak flux and fluence. It is possible that the true peak flux and fluence are higher.

The highest-energy bands around 800−950 keV, as shown in Fig. 1, have an increased number of counts during the GRB peak compared to lower-energy bands around 700−800 keV. This is also evident in the raw count spectrum at the peak time, $t_{\rm p}$, presented in Fig. 5. This could be due to an instrumental effect because of the high incident photon rate.

6. Conclusions

Our conclusions can be summarised as follows:

- GRBAlpha, a low-cost nano-satellite in a low-Earth orbit, detected the exceptionally bright long gamma-ray burst GRB 221009A without saturation, but affected by pile-up, providing light curves of the prompt emission in 13 energy bands from 80 keV to 950 keV.
- The peak flux in the 80−800 keV range (observer frame) is measured to be $F^{\rm p}_{\rm ph} = 1300^{+1200}_{-200}$ ph cm^{-2} s^{-1}, or $F^{\rm p}_{\rm erg} = 5.7^{+3.7}_{-0.7} \times 10^{-4}$ erg cm^{-2} s^{-1}, and for the wider extrapolated energy range of $0.9 - 8,690$ keV we obtain $F^{\rm p,bol}_{\rm erg} = 1.3^{+0.4}_{-0.2} \times 10^{-3}$ erg cm^{-2} s^{-1}.
- The peak isotropic-equivalent luminosity in the $92 - 920$ keV range (rest frame) was $L^{\rm p}_{\rm iso} = 3.7^{+2.5}_{-0.5} \times 10^{52}$ erg s^{-1}, and the bolometric peak isotropic-equivalent luminosity in the $1 - 10\,000$ keV range (rest frame) was $L^{\rm p,bol}_{\rm iso} = 8.4^{+2.5}_{-1.5} \times 10^{52}$ erg s^{-1} (4 s scale). Our measurement of $L^{\rm p,bol}_{\rm iso}$ is consistent with the Yonetoku relation between the rest-frame spectral peak energy and the peak luminosity of GRBs.
- The fluence in the 80−800 keV range of the first GRB episode, which lasted 300 s and was observable by GRBAlpha from 13:19:29.5 to 13:24:29.5 UTC on 2022 October 9, was measured to be $S = 2.2^{+1.4}_{-0.3} \times 10^{-2}$ erg cm^{-2} and $S^{\rm bol} = 4.9^{+0.8}_{-0.5} \times 10^{-2}$ erg cm^{-2} for the extrapolated range of 0.9−8690 keV. We infer from this extrapolated fluence that the isotropic-equivalent released energy of the first GRB episode was $E^{\rm bol}_{\rm iso} = 2.8^{+0.8}_{-0.5} \times 10^{54}$ erg in the $1 - 10\,000$ keV band (rest frame).
- It is possible that, due to the spectral evolution during the peaks of this GRB, as reported by Konus-WIND (Frederiks et al. 2023), the true peak flux, fluence, $L_{\rm iso}$, and $E_{\rm iso}$ may be higher than our obtained values. We cannot exclude that the GRBAlpha's detector was oriented near edge-on with respect to the GRB 221009A at the peak time,

which would also mean that the true values may be higher than our estimations.

Acknowledgements. We are thankful to Peter Veres and Stephen Lesage for discussions regarding the detection of this GRB by *Fermi*/GBM and other instruments and to Tomáš Plšek for discussions about MCMC and XSPEC. We are also thankful to Nozomu Kogiso, Maumu Yoneyama, Mizuki Moritaki, Tatsuya Kano and James W. Cutler for providing their SatNOGS stations for collecting GRBAlpha's telemetry. We acknowledge support by the KEP-7/2018 and KEP2/2020 grants of the Hungarian Academy of Sciences and SA-40/2021 of the Eötvös Loránd Research Network for satellite components and payload developments and the grant IF-7/2020 for providing the financial support for ground infrastructure. This research has been supported by the European Union's Horizon 2020 programme under the AHEAD2020 project (grant agreement n. 871158) and by the MUNI Award for Science and Humanities funded by the Grant Agency of Masaryk University. G.D. is supported by the Ghent University Special Research Funds (BOF) project BOF/STA/202009/040 and the Fonds Wetenschappelijk Onderzoek (FWO) iBOF project BOF20/IBF/124. This work was supported by the Internal Grant Agency of Brno University of Technology, project no. FEKT-S-20-6526. This research has been also supported by JSPS and HAS under Japan-Hungary Research Cooperative Program, JSPS KAKENHI Grant Number 17H06362, 19H01908, and 21KK0051. We are grateful to the Ministry of Education, Science, Research and Sport of the Slovak Republic for the support of the GRBAlpha mission.

References

Allison, J., Amako, K., et al. 2016, Nucl. Instrum. Methods Phys. Res. Sect. A, 835, 186
An, Z.-H., Antier, S., Bi, X.-Z., et al. 2023, Natl. Sci. Rev., submitted [arXiv:2303.01203]
Arnaud, K. A. 1996, in Astronomical Data Analysis Software and Systems V, eds. G. H. Jacoby, & J. Barnes, ASP Conf. Ser., 101, 17
Burns, E., Svinkin, D., Fenimore, E., et al. 2023, ApJ, 946, L31
de Ugarte Postigo, A., Izzo, L., Pugliese, G., et al. 2022, General Coordinates Network, 32648, 1
Dichiara, S., Gropp, J. D., Kennea, J. A., et al. 2022, ATel, 15650, 1
Dzhappuev, D. D., Afashokov, Y. Z., Dzaparova, I. M., et al. 2022, ATel, 15669, 1
Frederiks, D., Svinkin, D., Lysenko, A. L., et al. 2023, ApJ, 949, L7
Galgóczi, G., Řípa, J., Campana, R., et al. 2021, J. Astron. Telesc. Instrum. Syst., 7, 028004P
Górski, K. M., Hivon, E., Banday, A. J., et al. 2005, ApJ, 622, 759
Gotz, D., Mereghetti, S., Savchenko, V., et al. 2022, General Coordinates Network, 32660, 1
Hastings, W. K. 1970, Biometrika, 57, 97
Huang, Y., Hu, S., Chen, S., et al. 2022, General Coordinates Network, 32677, 1
Knoll, G. F. 2000, Radiation Detection and Measurement (New York: Wiley)
Kozyrev, A. S., Golovin, D. V., Litvak, M. L., et al. 2022, General Coordinates Network, 32805, 1
Lesage, S., Veres, P., Roberts, O. J., et al. 2022, General Coordinates Network, 32642, 1
Lesage, S., Veres, P., Briggs, M. S., et al. 2023, ApJ, 952, L42
Malesani, D. B., Levan, A. J., Izzo, L., et al. 2023, A&A, submitted [arXiv:2302.07891]
Mazets, E. P., Cline, T. L., Aptekar, R. L., et al. 2005, ArXiv e-prints [arXiv:astro-ph/0502541]
Mészáros, L., Pál, A., Werner, N., et al. 2022, in SPIE Conf. Ser., eds. J. W. A. den Herder, S. Nikzad, & K. Nakazawa, 12181, 121811L
Mitchell, L. J., Phlips, B. F., & Johnson, W. N. 2022, General Coordinates Network, 32746, 1
Oates, S. 2023, Universe, 9, 113
O'Connor, B., Troja, E., Ryan, G., et al. 2023, Sci. Adv., 9, eadi1405
Paciesas, W. S., Meegan, C. A., Pendleton, G. N., et al. 1999, ApJS, 122, 465
Pál, A., Ohno, M., Mészáros, L., et al. 2020, in Space Telescopes and Instrumentation 2020: Ultraviolet to Gamma Ray, eds. J. W. A. den Herder, S. Nikzad, & K. Nakazawa, SPIE Conf. Ser., 11444, 114444V
Piano, G., Verrecchia, F., Bulgarelli, A., et al. 2022, General Coordinates Network, 32657, 1
Pillera, R., Bissaldi, E., Omodei, N., La Mura, G., & Longo, F. 2022, ATel, 15656, 1
Planck Collaboration VI. 2020, A&A, 641, A6
Terasawa, T., Tanaka, Y. T., Takei, Y., et al. 2005, Nature, 434, 1110
Tiengo, A., Pintore, F., Vaia, B., et al. 2023, ApJ, 946, L30
Ursi, A., Panebianco, G., Pittori, C., et al. 2022, General Coordinates Network, 32650, 1
Veres, P., Burns, E., Bissaldi, E., et al. 2022, General Coordinates Network, 32636, 1
von Kienlin, A., Meegan, C. A., Paciesas, W. S., et al. 2020, ApJ, 893, 46
Řípa, J., Pál, A., Ohno, M., et al. 2022a, in Space Telescopes and Instrumentation 2022: Ultraviolet to Gamma Ray, eds. J. W. A. den Herder, S. Nikzad, & K. Nakazawa, SPIE Conf. Ser., 12181, 121811K
Řípa, J., Pal, A., Werner, N., et al. 2022b, General Coordinates Network, 32685, 1
Werner, N., Řípa, J., Pál, A., et al. 2018, in Space Telescopes and Instrumentation 2018: Ultraviolet to Gamma Ray, eds. J. W. A. den Herder, S. Nikzad, & K. Nakazawa, SPIE Conf. Ser., 10699, 106992P
Williams, M. A., Kennea, J. A., Dichiara, S., et al. 2023, ApJ, 946, L24
Xiao, H., Krucker, S., & Daniel, R. 2022, General Coordinates Network, 32661, 1
Yonetoku, D., Murakami, T., Tsutsui, R., et al. 2010, PASJ, 62, 1495

[1] Department of Theoretical Physics and Astrophysics, Faculty of Science, Masaryk University, Kotlářská 267/2, Brno 611 37, Czech Republic
e-mail: ripa.jakub@gmail.com
[2] Department of Physics, Graduate School of Advanced Science and Engineering, Hiroshima University, Higashi-Hiroshima, Japan
[3] Konkoly Observatory, Research Centre for Astronomy and Earth Sciences, Budapest, Hungary
[4] Eötvös Loránd University, Egyetem tér 1-3, Budapest, Hungary
[5] Wigner Research Centre for Physics, Konkoly-Thege Miklós út 29-33, Budapest, Hungary
[6] Spacemanic Ltd, Jablonec 110, 900 86 Jablonec, Slovakia
[7] Needronix Ltd, Ilkovičová 3, 812 19 Bratislava, Slovakia
[8] EDIS vvd., 04001, Košice, Slovakia
[9] Faculty of Aeronautics, Technical University of Košice, Košice, Slovakia
[10] Department of Radio Electronics, Faculty of Electrical Engineering and Communication, Brno University of Technology, Brno, Czech Republic
[11] Tokyo University of Science, Noda, Chiba, Japan
[12] Department of Physics, Nagoya University, Nagoya, Aichi, Japan
[13] Institute of Space and Astronautical Science, Japan Aerospace Exploration Agency, Kanagawa, Japan
[14] Institute of Earth Physics and Space Science (EPSS), Csatkai E. u. 6-8., 9400 Sopron, Hungary
[15] Department of Physics and Astronomy, Universiteit Gent, 9000 Ghent, Belgium
[16] School of Science, Kyoto University, Kyoto, Japan
[17] Department of Physics, Rikkyo University, Tokyo, Japan
[18] Department of Theoretical Physics, Institute of Physics, Budapest University of Technology and Economics, Műegyetem rkp. 3, 1111 Budapest, Hungary
[19] MTA-BME Quantum Dynamics and Correlations Research Group, Budapest University of Technology and Economics, Műegyetem rkp. 3, 1111 Budapest, Hungary
[20] Department of Earth and Space Science, Osaka University, Toyonaka, Osaka, Japan
[21] INAF – Istituto di Astrofisica Spaziale e Fisica Cosmica, Via A. Corti 12, 20133 Milano, Italy